A Sequential Plasma Focus

S. Lee

Abstract— **Recent shadowgraph studies suggest that a target disc placed downstream of the anode of a plasma focus may become an auxiliary anode producing a second focusing event when the current sheet climbs over it after the first focus event. A model is set up, with each event assumed to comprise three phases: an axial phase, a radial phase, and a radial extension or expanded column phase. This model is seen to produce the current dip, voltage spike, and high radial speeds characteristic of a plasma focus. With two separated discs acting as auxiliary anodes downstream of the usual anode, there are now three focus events with nine phases in the computation. The equations are written in generalized form in terms of n, so that an equation, for example, applicable to the first axial phase (nA, n = 1), is also applicable to the second (nA, n = 2) and third axial phase (nA, n = 3) by putting n = 1, 2, 3 successively in the equation. The results of the model indicate that each anode produces sequentially the current dip, voltage spike, and high radial speeds characteristic of the plasma focus. These computations suggest the possibility and design of a sequential or cascading plasma focus.**

I. Introduction

In a recent study, shadowgraphs [1] were taken of a flat disc target placed near and downstream of the anode of a plasma focus in order to assess whether the target disturbed the focusing dynamics. The term "focusing dynamics" here stresses the geometry of the focusing action as observed by some visual means, as distinct from its inferred properties of, for example, neutron ion beams [6] and X-ray yield. It was found that when the target was at a distance from the anode greater than the anode radius, there was no disturbance on the dynamics of the focus proper. This visual observation on focus dynamics is in general agreement with observations inferred from neutron and ion-beam emission characteristics [6]–[10]. However, it was further observed that after the focus proper the current sheet moved axially until it reached the disc target, whereupon the current sheet propagated around the disc target and pinched or focused again beyond it [1] onto the rod holding the disc target. It was as though the disc target had become a new "anode." The question then arose naturally whether a series of separated discs placed downstream of the main anode could each become sequentially a new anode to the advancing plasma current sheet, resulting in a series of sequential or cascading plasma focus. Practically, it would of course be necessary to "float" the discs in some manner so as not to have the rod holding the disc to obstruct the focus mechanism. Such a sequential plasma focus may have applications for the production of sequenced bursts of neutrons and soft X rays for neutron radiographic and soft X-ray cinematography.

In this paper a model is set up for the case of two discs to produce three sequential or cascading focus events. Each focus event [2] is divided into three parts: an axial run-down phase (denoted by A), a radial collapse phase (denoted by R), and a radial extension expanded column phase (denoted by C). There are altogether nine phases—$(1A, 1R, 1C, 2A, 2R, 2C, 3A, 3R, 3C)$—in this model with two auxiliary disc anodes, as depicted in Fig. 1.

In the axial phases $(nA, n = 1, 2, 3)$, a snow-plow model coupled to the circuit equation is found to be adequate to depict the gross dynamics in terms of speed and trajectory. In the radial phases $(nR, n = 1, 2, 3)$, a circuit-coupled slug model [2] with a slug [3] bounded by a shock front at position r_s and a magnetic piston at position r_p may be used to give a trajectory ending in a realistic end-point radius for the current sheet, or magnetic piston position at maximum compression. Following the maximum compression, experimental observations show that the plasma column breaks up into a large volume plasma. It is a characteristic of shadowgraphs taken at this time that no plasma column is visible, indicating that for the purpose of modeling, one may take as a first approximation the current path to be large and uniformly spread out as shown in phase $1C$ (Fig. 1(c)), where the current path linking the anode to the moving current sheet is depicted as flowing uniformly in a column. This is distinct from the case of phase $1A$ (Fig. 1(a)) or phase $1R$ (Fig. 1(b)), where all current paths are thin and indicated by a single arrow. In this model we also assume that phase $1R$ moves instantaneously into phase $1C$. Although this must be considered a deficiency of this model (resulting in too fast a voltage drop from peak voltage), it is not too far (from the viewpoint of gross dynamics) from experimental observations in which the transition from phase $1R$ to phase $1C$ is astonishingly rapid, particularly for small machines. For the expanded column phase, a snow-plow model coupled to the circuit equation is used similarly to the axial phase.

From phase $1C$, we depict in this model a transition to phase $2A$ (Fig. 1(d)), hence to phase $2R$ (Fig. 1(e)), phase $2C$ (Fig. 1(f)), phase $3A$ (Fig. 1(g)), phase $3R$ (Fig. 1(h)), and finally to phase 3C (Fig. 1(i)).

II. Theory

The equivalent circuit of the capacitor discharge of the plasma focus is shown in Fig. 2, with the external inductance depicted as L_0. The inductance of the plasma focus tube L_p in each of the 9 phases is listed below. Here, b is the radius

Manuscript received October 11, 1990; revised May 13, 1991. This work was supported by the Malaysian Ministry of Science, Technology, and the Environment under its Intensification of Research in Priority Areas (IRPA) programs.

The author is with the Nanyang Technological University, National Institute of Education, 469 Bukit Timah Road, Singapore 1025.

IEEE Log Number 9102550.

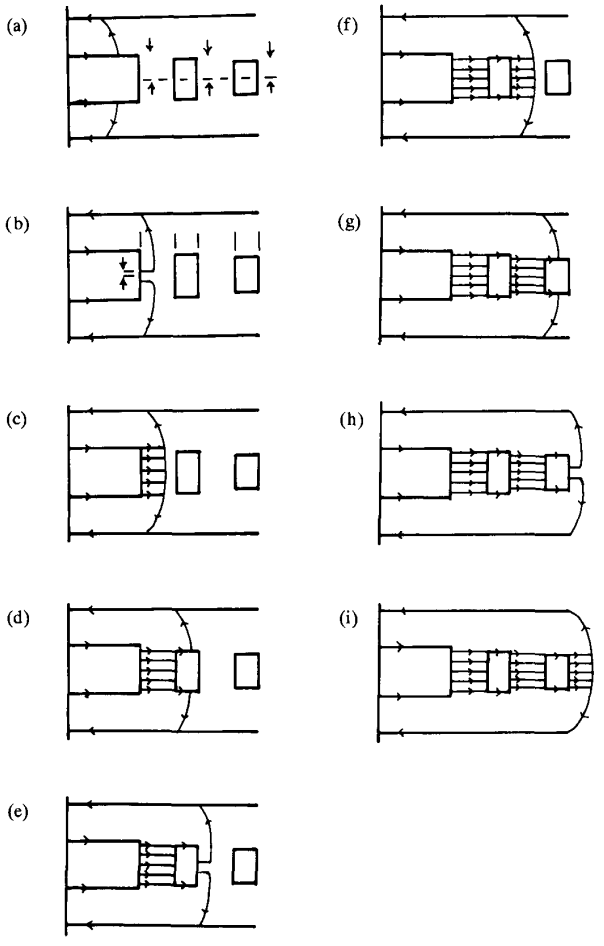

Fig. 1. The 9 phases of the sequential plasma focus model with 3 focus events. First focus event (n = 1): (a) phase 1A; (b) phase 1R; (c) phase 1C. Second focus event (n = 2): (d) phase 2A; (e) phase 2R; (f) phase 2C. Third focus event (n = 3): (g) phase 3A; (h) phase 3R; (i) phase 3C.

of the outer electrode, a_0, a_1, and a_2 are the radii of the inner electrode, first disc, and second disc, respectively, and z_0, z_1, z_2, z_3, and z_4 refer to the positions of the end of the anode and the ends of the discs, respectively (refer to Fig. 1). In the notation used in this paper, subscripts of 0, 1, 2, 3 are allowed. A quantity with a negative subscript has a value of zero.

For each of the 3 axial phases $nA(n = 1, 2, 3$, successively),

$$L_{nA} = \mu' \Big[(\ln c_{n-1})(z - z_{2n-4}) + (\ln c_{n-2})(z_{2n-4} - z_{2n-6}) + (\ln c_{n-3})(z_{2n-6}) + \frac{1}{4}(z_{2n-3} - z_{2n-4} + z_{2n-5} - z_{2n-6}) \Big] \quad (1)$$

(i.e., to obtain the inductance of phase $1A, L_{1A}$, put $n = 1$ in (1); to obtain the inductance of phase $2A, L_{2A}$, put $n = 2$ in (1); and likewise for L_{3A}), where $\mu' = \mu_0/(2\pi)$, where

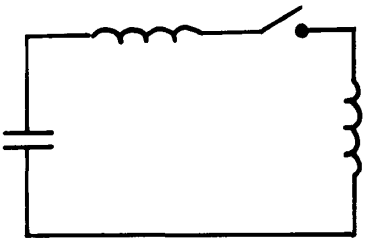

Fig. 2. Equivalent circuit of the sequential plasma focus. L_p is the plasma tube inductance.

μ_0 is the permeability of free space, and $c_n = b/a_n, z$ is the time-varying axial position of the current sheet).

For each of the 3 radial phases $nR(n = 1, 2, 3$ successively),

$$L_{nR} = \mu' \Big[(\ln \frac{b}{r_p}) z_f + (\ln c_{n-1})(z_{2n-2} - z_{2n-4}) + (\ln c_{n-2})(z_{2n-4} - z_{2n-6}) + (\ln c_{n-3})(z_{2n-6}) + \frac{1}{4}(z_{2n-3} - z_{2n-4} + z_{2n-5} - z_{2n-6}) \Big] \quad (2)$$

where $z_f = z - z_{2n-2}$.

For each of the 3 expanded column phases $nC(n = 1, 2, 3$ successively),

$$L_{nC} = \mu' \Big[(\ln c_{n-1})(z - z_{2n-4}) + (\ln c_{n-2})(z_{2n-4} - z_{2n-6}) + (\ln c_{n-3})(z_{2n-6}) + \frac{1}{4}(z - z_{2n-2} + z_{2n-3} - z_{2n-4} + z_{2n-5} - z_{2n-6}) \Big]. \quad (3)$$

For the axial phases [2] and the expanded column phases, the snow-plow equations require the mass loading. These and the corresponding axial-pointing $J \times B$ forces are listed as follows:

Mass loading for each of the 3 axial phases $nA(n = 1, 2, 3$ successively),

$$m_{nA} = \pi \rho_0 a_0^2 \Big[(c_0^2 - d_{n-1}^2)(z - z_{2n-4}) + (c_0^2 - d_{n-2}^2)(z_{2n-4} - z_{2n-6}) + (c_0^2 - d_{n-3}^2)(z_{2n-6}) \Big] \quad (4)$$

where $d_n = a_n/a_0$ and ρ_0 is the ambient mass density.

The corresponding force for each of the 3 axial phases is:

$$F_{nA} = \frac{\mu'}{2} I^2 (\ln c_{n-1}). \quad (5)$$

Mass loading for each of the 3 expanded column phases $nC(n = 1, 2, 3$, successively):

$$m_{nC} = \pi \rho_0 a_0^2 \Big[(c_0^2 (z - z_{2n-2} + (c_0^2 - d_{n-1}^2)(z_{2n-2} - z_{2n-4}) + (c_0^2 - d_{n-2}^2)(z_{2n-4} - z_{2n-6}) + (c_0^2 - d_{n-3}^2)(z_{2n-6}) \Big]. \quad (6)$$

The corresponding force for each of the 3 expanded column phases:

$$F_{nC} = \frac{\mu'}{2} I^2 \left[(\ln c_{n-1}) + \frac{1}{4} \right]. \tag{7}$$

III. The Equations Governing the Various Phases

A. The Axial Phases $nA(n = 1, 2, 3,$ Successively)

For each of these 3 axial phases, we may write two governing equations as follows:

$$\text{Axial Motion: } \frac{d}{dt}\left[m_{nA} \frac{dz}{dt} \right] = F_{nA} \tag{8}$$

where m_{nA} and F_{nA} are given in (4) and (5), respectively, and

$$\text{Circuit: } \frac{d}{dt}[(L_0 + L_{nA})I] = V_0 - \int I dt / C_0 \tag{9}$$

where L_{nA} is given by (1).

These two coupled equations are to be solved for z and I step-by-step, starting at $t = 0$ for the first axial phase, $n = 1$, with known starting conditions.

B. The Radial Phases $nR(n = 1, 2, 3,$ Successively)

For each of these 3 radial phases, we need 4 governing equations in order to follow the trajectories of r_s, the radial shock front, and r_p, the driving radial magnetic piston, together with the increasing length z_f of the open-ended pinching column and the current I. The equations of r_s and r_p for a constant current pinch have been discussed by Potter [3], and this slug-model has been modified for an elongating pinch with the circuit-coupled current [2] to give the following equations:

$$\text{Radial shock position: } \frac{dr_s}{dt} = -\left[\frac{\mu_0}{\rho_0}(\gamma + 1) \right]^{\frac{1}{2}} \frac{I}{4\pi r_p} \tag{10}$$

where γ is the ratio of the specific heat of the plasma;

$$\text{Axial elongation: } \frac{dz_f}{dt} = -\left(\frac{2}{\gamma + 1}\right) \frac{dr_s}{dt} \tag{11}$$

where $z_f = z - z_{2n-2}$;

$$\text{Radial piston position: } \frac{dr_p}{dt} = \frac{\frac{2}{\gamma+1} R \frac{dr_s}{dt} - \frac{r_p}{\gamma I}(1 - R^2)\frac{dI}{dt} - \left(\frac{1}{\gamma+1}\right)(1 - R^2)\frac{dz_f}{dt}\frac{r_p}{z_f}}{\left(\frac{\gamma-1}{\gamma}\right) + \frac{1}{\gamma}R^2} \tag{12}$$

where $R = r_s/r_p$; and

$$\text{Circuit: } \frac{d}{dt}[(L_0 + L_{nR})I] = V_0 - \int I dt / C_0 \tag{13}$$

where L_{nR} is given in (2).

C. The Expanded Column Phases $nC(n = 1, 2, 3,$ Successively)

For each of these 3 expanded column phases, we may write 2 governing equations as follows:

$$\text{Axial Motion: } \frac{d}{dt}\left[m_{nC} \frac{dz}{dt} \right] = F_{nC} \tag{14}$$

where m_{nC} and F_{nC} are given in (6) and (7), respectively; and

$$\text{Circuit: } \frac{d}{dt}[(L_0 + L_{nC})I] = V_0 - \int I dt / C_0 \tag{15}$$

where L_{nC} is given in (3).

IV. Normalization of Equations and Integration Procedure

As an aid to parametric analysis, the equations are normalized as follows:

$$\tau = \frac{t}{t_0} \quad \text{where } t_0 = \sqrt{L_0 C_0}$$
$$\iota = \frac{I}{I_0}$$

where $I_0 = V_0/\sqrt{L_0/C_0}$.

For axial phases and expanded column phases: $\zeta = \frac{z}{z_0}$

$$\text{For radial phases: } \kappa_s = \frac{r_s}{a_0}, \kappa_p = \frac{r_p}{a_0}, \zeta_f = \frac{z_f}{a_0}$$

where $z_f = z - z_{2n-2}$ for each phase $1R(n = 1), 2R(n = 2)$, and $3R(n = 3)$.

The normalized equations written as governing equations suitable for numerical integration are as given below.

A. The Axial Phases $nA(n = 1, 2, 3,$ Successively)

There are two governing equations for each phase. These are, in normalized form:

1) Axial Motion:

$$\frac{d^2\zeta}{d\tau^2} = \frac{\alpha^2 f_{n-1} \iota^2 - h_{n-1}\left(\frac{d\zeta}{d\tau}\right)^2}{\zeta_{2n-6} + h_{n-2}(\zeta_{2n-4} - \zeta_{2n-6} + h_{n-1}(\zeta - \zeta_{2n-4})} \tag{16}$$

where

$$f_{n-1} = \frac{\ln c_{n-1}}{\ln c_0}, h_{n-2} = \frac{c_0^2 - d_{n-2}^2}{c_0^2 - 1},$$
$$h_{n-1} = \frac{c_0^2 - d_{n-1}^2}{c_0^2 - 1}, d_{n-1} = \frac{a_{n-1}}{a_0},$$
$$d_{n-2} = \frac{a_{n-2}}{a_0}, \zeta_{2n-6} = z_{2n-6}/z_0, \zeta_{2n-4} = z_{2n-4}/z_0$$

and so on[1].

[1] In this paper, subscripts of 0, 1, 2, 3 are allowed. A quantity with a negative subscript has a zero value.

2) Circuit:

$$\frac{d\iota}{d\tau} = \left[(1 - \int \iota d\tau - \beta f_{n-1}\iota\frac{d\zeta}{d\tau}\right] / \left[1 + \beta\zeta_{2n-6} + \beta f_{n-2}(\zeta_{2n-4} - \zeta_{2n-6}) + \beta_1(\zeta_{2n-3} - \zeta_{2n-4} + \zeta_{2n-5} - \zeta_{2n-6}) + \beta f_{n-1}(\zeta - \zeta_{2n-4})\right] \quad (17)$$

where

$$f_{n-2} = \frac{\ln c_{n-2}}{\ln c_0}, \zeta_{2n-3} = z_{2n-3}/z_0.$$
$$\zeta_{2n-5} = z_{2n-5}/z_0, \beta_1 = \beta/4\ell n c_0.$$

In these two governing equations, the scaling parameters are α and β, where

$$\alpha^2 = t_0^2/t_a^2$$

scales the electrical characteristic time t_0 to the characteristic axial transit time $t_a^2 = [(4\pi^2\rho_0(c_0^2 - 1)z_0^2]/[(\ln c_0)(I_0/a_0)^2]$, and

$$\beta = \frac{\mu'(\ln c_0)z_0}{L_0}$$

scales the characteristic axial phase inductance $\mu'(\ln c_0)z_0$ to the external circuit inductance L_0.

To start the numerical step-by-step integration, we consider the axial phase of the first focus event; i.e., phase $1A$ (put $n = 1$). We may set [2] at the start:

$$(\tau)_0 = 0, \quad \left(\int \iota d\tau\right)_0 = 0, \quad (\iota)_0 = 0, \quad \left(\frac{d\iota}{d\tau}\right)_0 = 1,$$
$$(\zeta)_0 = 0, \quad \left(\frac{d\zeta}{d\tau}\right)_0 = 0, \quad \frac{d^2\zeta}{d\tau^2} = \alpha\sqrt{2/3}.$$

We may take increments of time $\Delta\tau = 0.001$ and use standard linear approximation methods to link $\int \iota d\tau$ with ι and $d\iota/d\tau$, and similarly ζ and $d\zeta/d\tau$ and $d^2\zeta/d\tau^2$ to obtain 4 additional equations (linear approximation). These 4 linear approximation equations, together with the governing equations (16) and (17), may then be used to solve for the 6 quantities: $\int \iota d\tau, \iota, d\iota/d\tau$ and $\zeta, d\zeta/d\tau, d^2\zeta/d\tau^2$ at each integration step. To start the integration of the phases $2A$ and $3A$, we use as starting values $\zeta = \zeta_{2n-3}$ and the final values of the preceding phase for $\tau, \int \iota d\tau, \iota, d\iota/d\tau, d^2\zeta/d\tau^2$. Each axial phase $nA(n = 1, 2, 3)$ is integrated until $\zeta = \zeta_{2n-2}$. For details of one simple scheme of integration, [2] may be used.

B. The Radial Phases $nR(n = 1, 2, 3$, Successively)

There are 4 governing equations for each radial phase. These are, in normalized form:

$$\text{Radial\_shock: } \frac{d\kappa_s}{d\tau} = -\frac{\alpha\alpha_1\iota}{\kappa_p} \quad (18)$$

where $\alpha_1 = \frac{[(\gamma+1)(c_0^2-1)]^{\frac{1}{2}}F}{2(\ell n c_0)}$ and $F = z_0/a_0$.

$$\text{Axial\_elongation: } \frac{d\zeta_f}{d\tau} = -(\frac{2}{\gamma+1})\frac{d\kappa_s}{d\tau} \quad (19)$$

where $\zeta_f = (z - z_{2n-2})/z_0$.

1) Radial Piston:

$$\frac{d\kappa_p}{d\tau} = \frac{(\frac{2}{\gamma+1}R'\frac{d\kappa_s}{d\tau} - \frac{1}{\gamma}\frac{\kappa_p}{\iota}(1 - R'^2)\frac{d\iota}{d\tau} - (\frac{1}{\gamma+1})\frac{\kappa_p}{\zeta_f}(1 - R'^2)\frac{d\zeta_f}{d\tau})}{(\frac{\gamma-1}{\gamma}) + (\frac{1}{\gamma}R'^2} \quad (20)$$

where $R' = \kappa_s/\kappa_p$.

2) Circuit:

$$\frac{d\iota}{d\tau} = \left[1 - \int \iota d\tau + \beta_f\iota\frac{\zeta_f}{\kappa_p}\frac{d\kappa_p}{d\tau} + \beta_f(\ln\frac{\kappa_p}{c_0})\iota\frac{d\zeta_f}{d\tau}\right] / \left[1 - \beta_f(\ln\frac{\kappa_p}{c_0})\zeta_f + \beta\zeta_{2n-6} + \beta f_{n-2}(\zeta_{2n-4} - \zeta_{2n-6}) + \beta f_{n-1}(\zeta_{2n-2} - \zeta_{2n-4}) + \beta_1(\zeta_{2n-3} - \zeta_{2n-4} + \zeta_{2n-5} - \zeta_{2n-6})\right] \quad (21)$$

where $\beta_f = \beta/(F\ell n c_0)$.

To start the integration of each radial phase, we use as starting values the following values of the corresponding preceding axial phase of τ, $\int \iota d\tau, \iota$, and $d\iota/d\tau$. Other initiating values are $\kappa_s = 1, \kappa_p = 1, \zeta_f = 0$ (or an inconsequential small value such as $\zeta_f = 0.00001$ to avoid the division of zero in (20)). The numerical integration proceeds for each case until $\kappa_s = 0$ at which point the minimum κ_p (an important quantity in experimental design) is reached.

C. The Expanded Column Phases $nC(n = 1, 2, 3$, Successively)

There are two governing equations for each expanded column phase. These are, in normalized form:

1) Axial Motion: See (22) below, where $e_{n-1} = (\ln c_{n-1} + \frac{1}{4}/\ln c_0, h = c_0^2/(c_0^2 - 1)$.

$$\frac{d^2\zeta}{d\tau^2} = \frac{\alpha^2 e_{n-1}\iota^2 - h(\frac{d\zeta}{d\tau})^2}{h_{n-3}\zeta_{2n-6} + h_{n-2}(\zeta_{2n-4} - \zeta_{2n-6}) + h_{n-1}(\zeta_{2n-2} - \zeta_{2n-4}) + h(\zeta - \zeta_{2n-2})} \quad (22)$$

2) Circuit:

$$\frac{d\iota}{d\tau} = \left[1 - \int \iota d\tau - \beta e_{n-1}\iota\frac{d\zeta}{d\tau}\right] / \Big[1 + \beta f_{n-3}\zeta_{2n-6} + \beta f_{n-2}(\zeta_{2n-4} - \zeta_{2n-6}) + \beta f_{n-1}(\zeta - \zeta_{2n-4}) + \beta_1(\zeta - \zeta_{2n-2} + \zeta_{2n-3} - \zeta_{2n-4} + \zeta_{2n-5} - \zeta_{2n-6})\Big]. \quad (23)$$

To start the integration of each expanded column phase $nC(n = 1, 2, 3)$, we use as starting values the following final values of the corresponding preceding radial phase $nR(n = 1, 2, 3)$: τ, $\int \iota d\tau, \iota$, and $\zeta = 1 + \zeta_f/F$ (renormalizing the value of ζ_f to z_0). We also use as a starting value the final value of $d\zeta/d\tau$ of the corresponding preceding axial phase $nA(n = 1, 2, 3)$.

The integration of each expanded column phase proceeds until $\zeta = \zeta_{2n-1}$, where for $n = 3, \zeta = \zeta_5$ may be taken as some convenient point such as $\zeta_5 = \zeta_4 + (\zeta_4 - \zeta_3)$.

V. Voltage Equations

Besides the measurement of current, another common and informative measurement which may readily be made of the plasma focus is the voltage V_p across the input of the focus. This may be computed, noting that:

$$V_p = \frac{d}{dt}(L_p I) \quad (24)$$

where we have assumed a purely inductive model, where L_p in the various phases are given by (1)–(3) successively.

The voltage equation is written for each of the 9 phases in normalized form [2], with $\nu = V_p/V_0$, where V_0 = initial voltage on capacitor, as follows:

Axial Phase $nA(n = 1, 2, 3$, successively):

$$\nu = \beta\frac{d\iota}{d\tau}\left[f_{n-3}\zeta_{2n-6} + f_{n-2}(\zeta_{2n-4} - \zeta_{2n-6}) + f_{n-1}(\zeta - \zeta_{2n-4}) + \frac{1}{4\ln c_0}(\zeta_{2n-3} - \zeta_{2n-4} + \zeta_{2n-5} - \zeta_{2n-6})\right] + \beta f_{n-1}\iota\frac{d\zeta}{d\tau}. \quad (25)$$

It is seen that the tube voltage contains two terms—the first being the product of displacement and rate of change of current, and the second, the product of current and speed. As the current peaks and stays near constant, the second, which we call the "speed term," dominates.

Radial Phase $nR(n = 1, 2, 3$, successively):

$$\nu = \beta\frac{d\iota}{d\tau}\left[f_{n-3}\zeta_{2n-6} + f_{n-2}(\zeta_{2n-4} - \zeta_{2n-6}) + f_{n-1}(\zeta_{2n-2} - \zeta_{2n-4}) + \frac{1}{4\ln c_0}(\zeta_{2n-3} - \zeta_{2n-4} + \zeta_{2n-5} - \zeta_{2n-6}) - \frac{\beta_f}{\beta}(\ln\frac{\kappa_p}{c_0})\zeta_f\right] - \beta_f\iota\left[(\ln\frac{\kappa_p}{c})\frac{d\zeta_f}{d\tau} + \frac{\zeta_f}{\kappa_p}\frac{d\kappa_p}{d\tau}\right]. \quad (26)$$

In the radial phase, the form of the voltage equation contains the two terms with the same dependence as in the axial phase. But in the radial phase the speed term has a much greater magnitude, especially the term involving the piston speed $d\kappa_p/d\tau$, since this term has κ_p in the denominator and has a larger effect as κ_p goes to smaller values.

Expanded Column Phase $nC(n = 1, 2, 3$, successively):

$$\nu = \beta\frac{d\iota}{d\tau}\left[f_{n-3}\zeta_{2n-6} + f_{n-2}(\zeta_{2n-4} - \zeta_{2n-6}) + f_{n-1}(\zeta - \zeta_{2n-4}) + \frac{1}{4\ln c_0}(\zeta - \zeta_{2n-2} + \zeta_{2n-3} - \zeta_{2n-4} + \zeta_{2n-5} - \zeta_{2n-6})\right] + \beta(f_{n-1} + \frac{1}{4\ln c_0})\iota\frac{d\zeta}{d\tau}. \quad (27)$$

VI. Results

Computations were carried out using this model with a view of designing a sequential or cascading focus system based on the 3-kJ plasma focus designated as the UNU/ICTP PFF [4]. The scaling parameters are $\alpha, \beta, \gamma, c_0, F, \zeta_1, \zeta_2, \zeta_3, \zeta_4, d_1$, and d_2. In order to reduce the large number of possible combinations to arrive at a combination which will provide a good focusing characteristic (large voltage spike, significant current dip) for all 3 sequential focus events, we note that the speed scaling [4] in both the axial and radial phases is dependent on the factor $(I/a)/\sqrt{\rho_0}$, so that it is necessary to maintain the value of (I/a) during each of the sequential focusing events. Thus basically we adjust the scaling parameters from the values of the UNU/ICTP PFF so that the first focus of the sequential focus occurs earlier than the focus of the UNU/ICTP PFF. Also, to maintain the value of (I/a), the auxiliary anodes are designed with radii a_1 and a_2 a little less than a_0.

Thus whereas the UNU/ICTP PFF was numerically optimized with the parameters $\alpha = 1.26, \beta = 0.36, F = 16.8, c_0 = 3.37$, and $\gamma = 5/3$, the sequential plasma focus is redesigned with $\alpha = 1.7, \beta = 0.27, F = 12, c_0 = 3.37, \gamma = 5/3$, and with $\zeta_1 = 1.083, \zeta_2 = 1.167, \zeta_3 = 1.25, \zeta_4 = 1.333, d_1 = 0.85$, and $d_2 = 0.7$.

These parameters correspond to the sequential plasma focus operating with the following conditions: $V_0 = 15\text{kV}, \text{C}_0 = 30\mu\text{F}, \text{L}_0 = 110\text{nH}, \text{a}_0 = 1\text{cm}, \text{z}_0 = 12\text{cm}, \text{z}_1 = 13\text{cm}, \text{z}_2 = 14\text{cm}, \text{z}_3 = 15\text{cm}, \text{z}_4 = 16\text{cm}, \text{a}_2 = 0.85\text{cm}, \text{a}_3 = 0.7$ cm, and pressure = 1 torr in deuterium. (Due to current and mass shedding [4] that is not included in the present modeling, the actual operational pressure would be closer to 3 torr.)

The 3-event, 9-phase model was computed with the computation numerically carried out in the sequence $1A, 1R, 1C, 2A, 2R, 2C, 3A, 3R$, and $3C$ using the normalized equations (16) and (17) for the axial phases, (18)–(21) for the radial phases, and (22) and (23) for the expanded column phases. The voltage was also computed using (25)–(27).

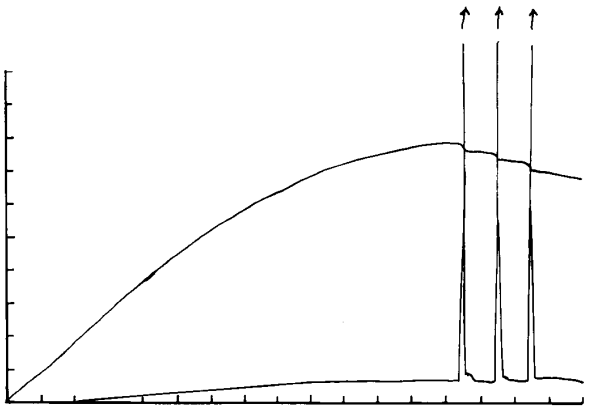

Fig. 3. Current ι and voltage ν for the sequential focus, with $\alpha = 1.7$, $\beta = 0.27$, $F = 12$, $c = 3.37$, $\gamma = 5/3$, $\zeta_1 = 1.083$, $\zeta_2 = 1.167$, $\zeta_3 = 1.25$, $\zeta_4 = 1.333$, $d_1 = 0.85$, and $d_2 = 0.7$. To help identify the 9 phases, their time intervals are as follows: phase $1A$: $\tau = 0 - 1.335$; phase $1R$: $\tau = 1.335 - 1352$ (first voltage spike); phase $1C$: $\tau = 1.352 - 1.369$; phase $2A$: $\tau = 1.369 - 1.437$; phase $2R$: $\tau = 1.437 - 1.449$ (second voltage spike); phase $2C$: $\tau = 1.449 - 1.473$; phase $3A$: $\tau = 1.473 - 1.539$; phase $3R$: $\tau = 1.539 - 1.548$ (third voltage spike); and phase $3C$: $\tau > 1.548$.

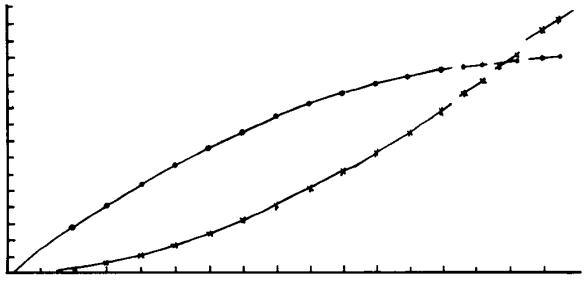

Fig. 4. Axial position ζ and axial speed during the phases $1A$, $2A$, $3A$ and $1C$, $2C$, $3C$ for the sequential focus with parameters given in the caption of Fig. 3. The three gaps represent the three phases $1R$, $2R$, $3R$, results of which are given separately in Fig. 5(a)–(c).

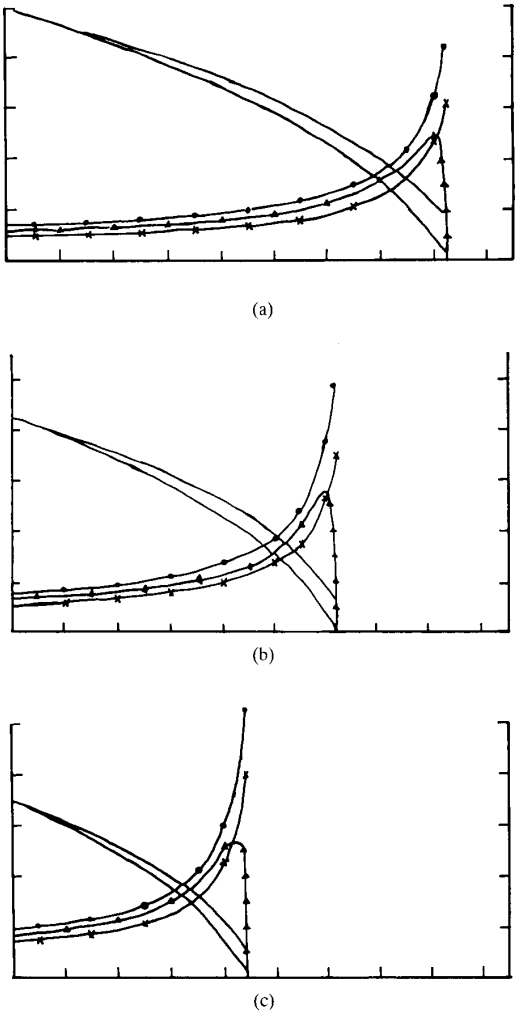

Fig. 5. (a) Radial phase $1R$: trajectories of radial shock (κ_s) and radial piston (κ_p) for the sequential focus with parameters the same as in the caption of Fig. 3. Also given are the radial shock speed $d\kappa_s/d\tau$ (•), radial piston speed $d\kappa_p/d\tau$ (△), and focus column elongation rate $d\zeta_p/d\tau$ (×). (b) Radial phase $2R$: trajectories of radial shock (κ_s) and radial piston (κ_p) for the sequential focus with parameters the same as in Fig. 3. Also given are the radial shock speed $d\kappa_s/d\tau$ (•), radial piston speed $d\kappa_p/d\tau$ (△), and focus column elongation rate $d\zeta_p/d\tau$ (×). (c) Radial phase $3R$: trajectories of radial shock (κ_s) and radial piston (κ_p) for sequential focus with parameters the same as in Fig. 3. Also given are the radial shock speed $d\kappa_s/d\tau$ (•), radial piston speed $d\kappa_p/d\tau$ (△), and focus column elongation rate $d\zeta_p/d\tau$ (×).

The results are presented in Figs. 3–5. In Fig. 3, the current ι and voltage ν waveforms are presented. The current reaches a peak value of 0.787 at $\tau = 1.335$ at the end of phase $1A$, just before the start of phase $1B$ (see Fig. 4). During this phase $1R$, it drops to 0.765 or by 2.8% of the peak value, with the steepest part of the drop occurring at $\tau = 1.3515$. This steep drop of current corresponds to the peak voltage which spikes up to a value of $\nu = 8.28$, corresponding to a piston speed of 5.9 (see Fig. 5(a)) scaled to a characteristic speed of z_0/t_0. These three effects—namely, the current dip, the voltage spike (contributed mainly by the term $(d\kappa_p/d\tau)/\kappa_p$) (see voltage equation [26]), and the fast radial piston speed—are the "classic" characteristics of a plasma focus. During this radial phase a further, though smaller, contribution to the voltage spike (see (26)) is the high axial elongation speed of up to 12.6.

After the radial phase $1R$, our model allows for a radial extension or expanded column phase $1C$ during which the current remains practically constant at $I = 0.7648$ (see Fig. 3), dropping gradually to 0.757. The tube voltage drops to a value of 0.347, slightly above the $1A$ final value of 0.27. This higher value is due to the extra inductance term of $\frac{1}{4}\mu' z_f$ (see (3) and (27)) during the $1C$ phase. The axial speed stays practically constant (see Fig. 4) at 1.23, only slightly higher than the final axial speed of phase $1A$. Phase $1C$ moves on to phase $2A$, characterized by an almost constant current, slightly lower tube voltage, and slightly higher axial speed.

At the end of phase $2A$ the second radial collapse phase $2R$ occurs, with the current dipping noticeable by another 2.5%, from 0.757 to 0.738 in a short time interval of 0.012 (see Fig. 3). The voltage spikes up to 9.14 at $\tau = 1.45$ contributed

mainly by the high piston speed. This radial collapse again has all three classic indications of a plasma focus. The phases $2C$ and $3A$ have similar characteristics as the earlier axial phases: almost constant current, tube voltage, and axial speed.

At the end of phase $3A$, the third radial collapse phase $3R$ occurs, this time with a current dip of 2.5%, from 0.729 to 0.711, and a voltage spike of peak value 10.5, corresponding to a peak piston speed of 10.1 at $\tau = 1.55$. This focus event also has all three characteristics of a strong plasma focus. Indeed, the parameters having been adjusted so that this third focus in the sequential series occurs at $\tau = 1.55$, and moreover, with the relevant anode having a radius of 0.7 of the main anode, this assures that there is an ample near-peak current so that the value of (I/a_2) ensures the highest radial speed and largest voltage spike during phase $3R$ of all three focus events.

Following this radial phase $3R$, we follow the plasma dynamics through one more axial phase $3C$ to bring the voltage down to the small values which characterize an axial phase. The current gradually drops further during this phase.

Fig. 5(a)–(c) shows the results of the computation on the radial phases $1R, 2R$, and $3R$. These three graphs fill-in the three gaps in Fig. 4. On an expanded time scale, each of the three graphs of Fig. 5(a)–(c) show the shock trajectory κ_s and piston trajectory κ_p and the corresponding speed graphs $d\kappa_s/d\tau$ and $d\kappa_p/d\tau vs\tau$. Also displayed is the elongation speed $d\zeta_f/d\tau$.

In Fig. 5(a), showing the results for the first of the radial phases, the plasma starts pinching at $\kappa_s = \kappa_p = 1$ at the time $\tau = 1.335$. Up to $\tau = 1.347$, the speeds $d\kappa_s/d\tau, d\kappa_p/d\tau$, and $d\zeta_f/d\tau$ have risen to values of about 4 from initial values of about 1 (in a time interval of 0.012). But in the next smaller time interval of 0.003 from 1.347 to 1.350, the values of $d\kappa_s/d\tau$ and $d\zeta_f/d\tau$ have risen to over 16 and 12, respectively, while the value of $d\kappa_p/d\tau$ has risen to 9 and then drops sharply to 0 in the very last instant as the radially imploding shock front goes on axis.

The very large voltage spike of $1R$ of Fig. 3 is due to the large value attained by $d\kappa_p/d\tau$ in the small interval of 0.003 from 1.345 to 1.350, coupled to the decreasing value of κ_p during this short interval of time.

The feature of $\kappa_p \cdot \kappa_s$ and the speeds $d\kappa_s/d\tau, d\kappa_p/d\tau$, and $d\zeta_f/d\tau$ follow the same pattern for the other 2 radial phases, $2R$ and $3R$.

It may be commented that the radial collapse speed and the voltage spike, say of $1R$, coming out of these computations are too large when compared with voltage measurements on a plasma focus. There are two mechanisms contributing to this effect. First, the effect of current-shedding and mass-shedding. About 0.7 of the capacitance current flows in the plasma in both the axial and radial phases. Also in the axial phase the effective mass loading on the current sheath is known [5] to be considerably below that expected from the operational density. This reduced mass loading or mass-shedding effect is due primarily to the severe canting of the current sheath in the axial phase. In the radial phase, however, the mass-shedding effect is not expected to operate. Thus to reflect the similar current-shedding but different mass shedding, the model could use a differential pressure (density) method with a considerably larger density in the radial phase than in the axial phases. This would reduce the computed radial speeds and voltage spike.

For the second mechanism, it would be correct to say that because the slug model assumes instantaneous signal communication [3] between the shock front and piston, this leads to the computed exceedingly large values. If we consider the communication delay due to the finite small disturbance speed between the piston and shock front (of the order of 0.3 mm/μs or in the nondimensionless units of these calculated 0.1 units of distance in 0.002 units of time), then because in the slug model the piston pressure drives the shock front and the motion of the shock front creates volume for the piston to move into, a communication delay of 0.002 or 0.003 in time between the piston and shock front would mean that the shock front would at any instant feel the considerably smaller pressure of the piston at an earlier time, and likewise the piston would feel the effect of the shock front at an earlier position. This delay effect, if incorporated into the model, would considerably slow down both the shock front and piston as they near the axis, and hence also reduce the voltage spike.

Operating the sequential focus in deuterium, a neutron pulse may be expected with each focus. It would be necessary to "float" the auxiliary anode in some manner so that the axial region beyond the auxiliary anode is unobstructed to the focus action. The presence of the target holder in all earlier target experiments obstructed the focus action so that multiple focus action from the targets was not observed [6]–[10]. It may also be necessary to use hollow auxiliary anodes; i.e., with a hole in the center in order not to disturb the deuteron beam-gas target mechanism responsible for a proportion of the fusion reaction in a plasma focus.

As mentioned in the introduction, such a sequential plasma focus may have applications in the production of sequenced bursts of neutrons and soft X-ray. For a greater number of pulses—i.e., a longer sequence—it may be advantageous to use a flat-top current pulse from an LC network discharge.

VII. Conclusion

Dividing a plasma focus event into three phases of which the first, the axial phase A, is followed by a radial phase R, which is then followed by an expanded column axial phase C, enables the plasma focus event to be computed with all the main features observed experimentally; in particular, the current, voltage, and speed characteristics during the axial phases A and C, and the voltage spike, current dip, and large radial collapse speed during the radial R phase. By the introduction of two auxiliary anodes, the model demonstrates that sequential or cascading plasma focus events may be achieved—each event exhibiting the three phases of A, R, and C, including all the dynamics and voltage and current characteristics of the two radial phases A and C and the radial R phase. Design parameters based on a 3-kJ focus such as the UNU/ICTP PFF [4] have also been suggested in these computations.

ACKNOWLEDGMENT

The idea for this work originated during the ICTP Training Program on Plasma and Pulse Technology carried out at the University of Malaya in 1990. Some aspects of this paper were completed at the ICTP (Trieste, Italy) in 1991.

REFERENCES

[1] S. Lee *et al.*, "Effect of targets on plasma focus dynamics," *IEEE Trans. Plasma Sci.*, vol. 18, pp. 1028–1032, 1990.
[2] S. Lee, "A plasma focus model yielding trajectory and structure," in *Radiation in Plasmas*, B. McNamara, Ed. World Scientific, 1984, pp. 967–977; see also, S. Lee *et al.*, "Technology of the plasma focus," in *Laser and Plasma Technology*. World Scientific, 1985, pp. 387–420.
[3] D. E. Potter, *Nucl. Fusion*, vol. 18, p. 813, 1978.
[4] S. Lee *et al.*, "A simple facility for the teaching of plasma dynamics and plasma nuclear fusion," *Amer. J. Phys.*, vol. 56, pp. 62–68, 1988.
[5] S. P. Chow, S. Lee, and B. C. Tan, "Current sheath studies in a co-axial plasma focus gun," *J. Plasma Phys.*, vol. 8, pp. 21–31, 1972.
[6] S. P. Moo, C. K. Chakrabarty, and S. Lee "An investigation of the ion beam of a plasma focus using a metal obstacle and deuterated target" *IEEE Trans. Plasma Sci.*, vol. 19, p. 515, 1991.
[7] K. Steinmetz and K. Hubner, *Nucl. Fusion*, vol. 22, p. 25, 1982.
[8] A. Bernard *et al.*, *Nucl. Instrum. Meth.*, vol. 145, p. 191, 1977.
[9] M. Sadowski, Z. Zebowski, E. Rydygier, and J. Kucinski, "Ion emission from plasma focus facilities," *Plasma Phys. Control. Fusion*, vol. 30, p. 763, 1988.
[10] P. Cloth and H. Conrads, "Neutronics of a dense plasma focus—an investigation of a fusion plasma," *Nucl. Sci. Eng.*, vol. 62, p. 591, 1977.

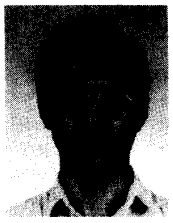

S. Lee received the B.Sc. and M.Sc. degrees in physics from the University of Malaya, Kuala Lumpur, Malaysia, in 1964 and 1966, respectively, and the Ph.D. degree from the Australian National University in 1970.

He was Professor of Applied Physics, Leader of the Research Groups in Plasma and Pulse Technology, and Head of the Physics Department of the University of Malaya. He is now with the Nanyang Technological University, National Institute of Education, Singapore. He was an Alexander Von Humboldt Research Fellow at Kernforschungsanlage, Juelich, Germany (1975–1976), a Commonwealth Academic Staff Fellow at the Imperial College, London (1981–1982), and a Visiting Professor and United Nations University Special Fellow at Flinders University of South Australia (1986–1987). He is the Founder President of the Asian–African Association for Plasma Training, the Far Eastern Representative of the International Centre for Theoretical Physics, and an ardent advocate and implementor of South–South technology creation and transfer, especially in plasma, fusion, laser, and pulse technology.

Dr. Lee is a Chartered Physicist and Fellow of the Institute of Physics (UK), and a Vice President of the Malaysian Institute of Physics.